Qubit fidelity of a single atom transferred among the sites of a ring optical lattice

Shi Yu,[1,2,3] Peng Xu,[1,2,*] Min Liu,[1,2] Xiaodong He,[1,2] Jin Wang,[1,2] and Mingsheng Zhan[1,2,†]

[1]*State Key Laboratory of Magnetic Resonance and Atomic and Molecular Physics, Wuhan Institute of Physics and Mathematics, Chinese Academy of Sciences–Wuhan National Laboratory for Optoelectronics, Wuhan 430071, China*

[2]*Center for Cold Atom Physics, Chinese Academy of Sciences, Wuhan 430071, China*

[3]*University of Chinese Academy of Sciences, Beijing 100049, China*

(Received 6 October 2014; published 22 December 2014)

We demonstrate the transfer of a single atom in a ring optical lattice with the aid of an auxiliary moving tweezer and investigate the influences on fidelity of the qubit encoded in the atom. When the tweezer has deeper trap depth and moves across the lattice, it is observed that an atom in one site follows the movement. The transfer efficiency of one atom to the destination site reaches up to 95%. This scheme is suitable for scalable quantum registers because of no influence on the other sites. We obtain atomic qubit fidelity during the transfer process by using quantum state tomography. Extracted fidelity indicates that the eigenstate is well preserved, while the superposition state is influenced. In combination with spin-echo measurement, dephasing mechanisms in this process are analyzed and discussed in detail. Loss of qubit fidelity is found to result from heating effects induced by this process and pointing instabilities of the trap laser. Our results pave the way for quantum computation with single atoms trapped in a scalable optical lattice.

DOI: 10.1103/PhysRevA.90.062335 PACS number(s): 03.67.Lx, 37.10.Jk, 42.50.Ct

I. INTRODUCTION

Fundamental ingredients of an architecture for quantum computation include initialization and readout of scalable quantum registers, and gate operation of single- and multiqubits [1–3]. For quantum computing with neutral atoms, qubits are encoded in the internal states of single atoms, and each atom is confined in one site of an optical lattice. Quantum registers are initialized by loading single atoms into the optical lattice from cold or ultracold atom ensembles [4,5]. The readout is realized by detecting and addressing the lattice with single site resolution [6–9]. Meanwhile, by manipulating the hyperfine states with microwave or stimulated Raman transitions, single-qubit operation is easy to implement [4,10–12]. Recently, two-qubit gates have been performed with single atoms in two neighbor tweezers utilizing Rydberg blockade [13–15], and with many pairs of atoms in the lattices via controlled ground-state collisions [16–18]. However, quantum gate between arbitrary pairs of qubits in scalable registers has not been demonstrated.

Scalability is an important issue in quantum computation. As proposed in Ref. [19], quantum computation architecture with cold atoms in optical lattices needs gate operation between arbitrary qubits. One basic requirement for the operation is to transport atoms from remote sites into the interaction range. Several transport schemes have been implemented, including spin-dependent transportation in a standing-wave optical lattice [17,20,21], "optical conveyor belt" [22], and alternate transfer between two moving tweezers [23]. In addition, a transport technique has also been demonstrated in small atomic ensembles [24–26]. Nevertheless, in a real scalable quantum register, the lattice structures are normally created by superimposing standing-wave laser fields along different directions or using diffractive elements to replicate laser beams [27–29]. It is difficult to separately alter each site condition, including its location and depth, especially in a huge quantum register. Therefore, controlled transfer of single atoms among the selected sites without changing the whole lattice is a key step for a scalable quantum system.

A similar multizone ionic array architecture has been usually adopted for scalable quantum information processing with trapped ions, where ion shuttling between storage and interaction regions has been investigated for over ten years [30–35]. The main requirements and challenges include high success probability, maintained vibrational ground state and qubit fidelity, and minimal transport time.

In this paper we study two issues, i.e., the transfer efficiency of an atom from one site to another without the influence on the registers and the fidelity of the qubit during the transfer process. First, a ring optical lattice with three to six sites is created using a spatial light modulator (SLM). Then, we experimentally demonstrate the transfer of a single ^{87}Rb atom in the ring optical lattice with an auxiliary moving optical tweezer. As pointed out in Ref. [19], by just changing the potential depth of the moving tweezer, the atom in one site follows the tweezer due to the deeper depth when the tweezer crosses the site. This scheme is suitable for scalable quantum registers because of no influence on other sites. It does not require changing the lattice itself, and does not affect coherence properties of single atoms in a neighboring site. Finally, we reconstruct the density matrix and extract the qubit fidelity by using quantum state tomography during the transfer process. In combination with spin-echo measurement, we analyze and discuss influence mechanisms.

The paper is organized as follows. In Sec. II the experimental setup and results are described. We demonstrate the transfer of single atoms among the sites and measure qubit fidelity and coherence time. In Sec. III we theoretically analyze dephasing mechanisms and the influences on qubit fidelity during the transfer process. Finally, in Sec. IV the major findings and the overall performance of our transfer scheme are discussed and summarized.

*etherxp@wipm.ac.cn
†mszhan@wipm.ac.cn

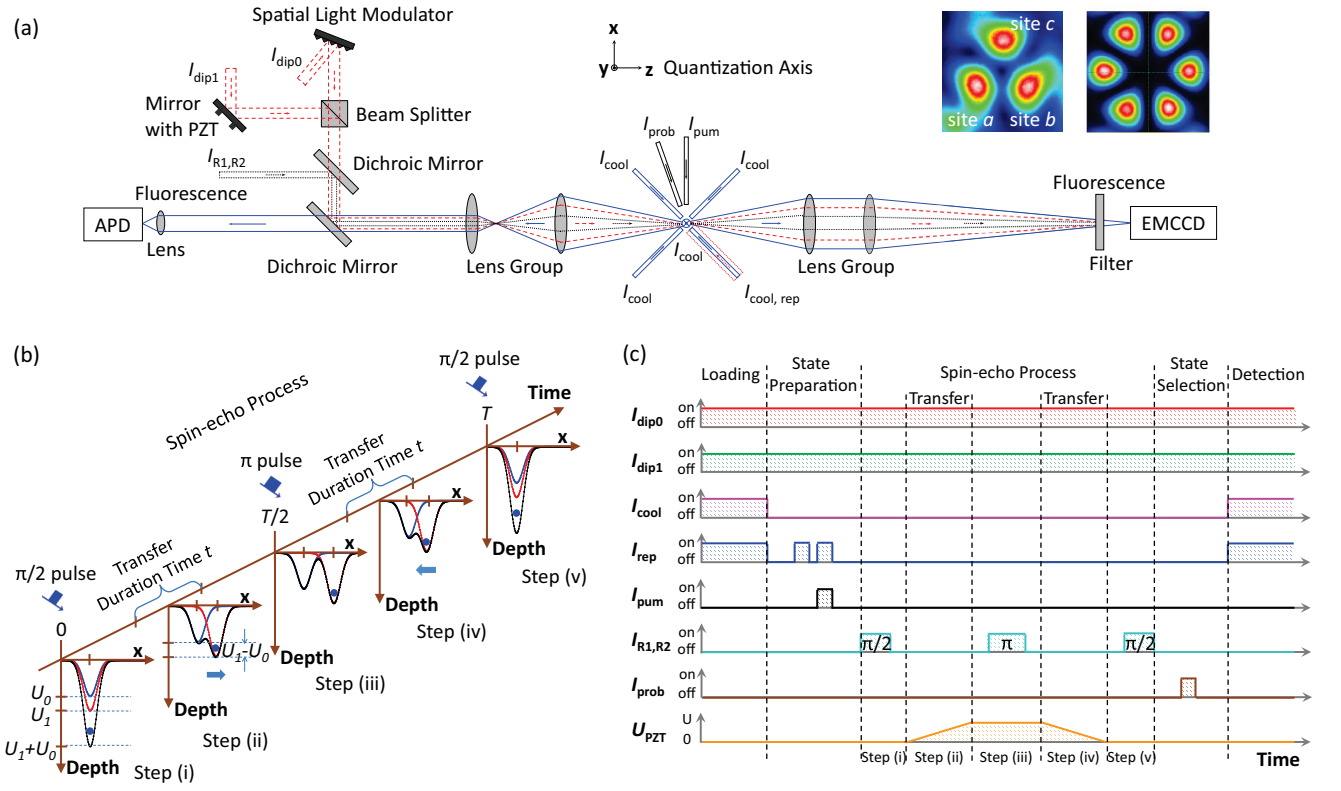

FIG. 1. (Color online) (a) Schematic of experimental setup. A spatial light modulator is applied to generate a ring optical lattice (I_{dip0}). The inset shows two images of the lattices with three sites and six sites. A moving optical tweezer (I_{dip1}) is reflected from a piezoelectrical transducer (PZT) mirror and combined with the lattice. Fluorescence of single atoms is detected simultaneously with an avalanche photodiode (APD) and an electron multiplying charge coupled device (EMCCD) camera. (b) Experimental investigation of qubit fidelities and coherence properties during the transfer process. Atom is initially located in the overlap between the static trap and the moving tweezer. It is transferred to another location for a duration time t, and then transported back under the same conditions. (c) Experimental time sequence for the transfer investigation. The moving tweezer (I_{dip1}) is initially overlapped with the static trap (I_{dip0}) and always switched on. Once one atom is loaded in the combined trap, we switch off the magneto-optical trap (I_{cool} and I_{rep}) and prepare a single qubit in the initial state (I_{rep} and I_{pum}). Following the movement of the tweezer (U_{PZT}), the atom is transferred to the destination and then transported back. During the transfer process, a spin-echo technique that consists of $\pi/2 - \pi - \pi/2$ Raman pulses ($I_{R1,R2}$) is applied. Finally, the state-selective detection (I_{prob}) is performed for analysis of coherence properties.

II. EXPERIMENTAL MEASUREMENTS AND RESULTS

A. Transfer in a ring optical lattice

Our experimental setup is depicted in Fig. 1(a) and has been described in detail elsewhere [12,36,37]. A laser beam with 830 nm wavelength is tightly focused to a waist of 2.1 μm in the center of the ^{87}Rb magneto-optical trap (MOT). Based on a "collisional blockade" mechanism [38], single atoms are localized in the resulting far-off-resonance trap (FORT). In order to generate a ring optical lattice, a computer controlled SLM is used to transform a single Gaussian beam (I_{dip0}) with first-order diffraction efficiency of 40% [27]. Our holograms contain phases of the superposed Laguerre-Gaussian modes. They have radial mode number $p = 0$ and azimuthal mode numbers l_1 and l_2. The corresponding intensity patterns consist of $|l_1 - l_2|$ petals, with each petal as an optical dipole trap. A moving tweezer is generated by using another FORT beam (I_{dip1}) which is reflected from a piezoelectrical transducer (PZT) mirror and combined with the lattice by a beam splitter. The lifetime of a trapped atom is about 10 s in the absence of any near-resonant light. Laser induced fluorescence is collected with two groups of lenses on both sides of the vacuum chamber. One part is coupled into a fiber and detected with an avalanche photodiode (APD). By adjusting the position of the lenses, we collect the fluorescence from the desired original site to discriminate whether one atom is trapped or not. The other part is imaged onto an electron multiplying charge coupled device (EMCCD) camera. During the transfer process, in order to prevent collisions between two atoms in one trap, it is ensured that no atom is loaded from the MOT in the target site. Since the APD has a limited visual field, the EMCCD camera is used in parallel to monitor the whole lattice. It is valuable to detect the initial absence and the final presence of one atom in the destination.

A bias magnetic field of $B_0 = 2$ G is applied along the z axis. We define the logical states as $|0\rangle \equiv |F = 1, m_F = 0\rangle$ and $|1\rangle \equiv |F = 2, m_F = 0\rangle$. A qubit can be initialized in the state $|1\rangle$ using an optical pumping laser beam (I_{pum}). Single-qubit manipulations between the states $|0\rangle$ and $|1\rangle$ are performed by two-photon stimulated Raman transitions. Raman laser beams (I_{R1}, I_{R2}) are red-detuned by about 60 GHz from the D_1 transition and separated by 6.8 GHz utilizing

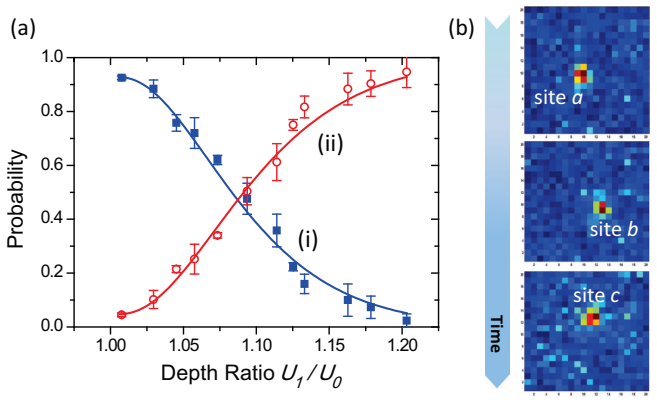

FIG. 2. (Color online) (a) Transfer efficiencies as a function of the depth ratio between the moving tweezer and the static trap. Solid square data (i) are the probabilities of single atoms remaining in the static trap. Open circle points (ii) represent the efficiencies of transferring to another location by the moving tweezer. All data are averaged over 100 single atom events. We fit the points according to Eq. (2) depicted in the text. It gives a maximum value of $95 \pm 5\%$ when the depth ratio is larger than 1.2. (b) Transfer of one atom in a ring optical lattice of three sites. After being initially trapped in site a, the atom is transported to site b and site c in sequence. The fluorescence images are captured by the EMCCD camera with an exposure time of 50 ms.

an acoustic-optical modulator. They propagate along the quantization axis and are focused in the location of single atoms. For the state-selective detection, a probe laser beam (I_{prob}) is applied to push out single atoms in the state $|F = 2\rangle$. However, atoms in the state $|F = 1\rangle$ are not influenced by this laser and remain in the trap. Coherence properties of internal states are therefore measured and investigated. In our previous work [12], the spin relaxation time of $T_1 = 830$ ms for the trap $U/k_B = 0.7$ mK was reported. Resulting from the spontaneous Raman scattering of photons from the trap laser, it is prolonged for the lower potential depth. Meanwhile, the inhomogeneous dephasing time of $T_2^* = 1.4$ ms was extracted from Ramsey spectroscopy. It originates from the energy distribution of trapped atoms and can be reversed via spin echo. From the decrease of the visibilities at different spin-echo time, the homogeneous dephasing time T_2' was obtained.

In our experiment, after trapping a single atom in one determined site of the lattice, an auxiliary tweezer crosses the site and moves to another location. The atom follows the moving tweezer due to the deeper depth. In order to acquire high transfer efficiency, we gradually increase the depth of the moving tweezer $U_1 = cU_0$ ($c \geqslant 1$). Here, U_0 is constant, representing the potential depth of the static trap at the site of the lattice. As shown in Fig. 2(a), transfer efficiencies increase with the depth ratio between two traps. Similarly, for the transport of small atomic ensembles in [26], the splitting ratios between transferred and untransferred atoms are dependent on the trap depth. In our conditions, the maximum efficiency is $95 \pm 5\%$ when the ratio satisfies $c \geqslant 1.2$. We assume that an atom with energy E smaller than the differential depth $\Delta U = U_1 - U_0$ is completely trapped in the moving tweezer. The energy distribution of single atoms in the dipole trap obeys a Boltzmann distribution, which gives the probability as [39]

$$P_{\mathrm{E}<\Delta\mathrm{U}} = 1 - \left[1 + \eta + \tfrac{1}{2}\eta^2\right]e^{-\eta}, \tag{1}$$

where η is defined as $\eta = (c-1)\,U_0/k_B T_a$, and T_a is the temperature of single atoms. In addition, an atom with larger energy partially follows the moving tweezer. We define the corresponding probabilities of single atoms presented in the static trap and the moving one as $A(1 - P_{\mathrm{E}<\Delta\mathrm{U}})$ and $(1 - A)(1 - P_{\mathrm{E}<\Delta\mathrm{U}})$, where A is a scaling factor. As a consequence, the summations of probabilities in the static and moving traps are given by

$$P_s = A\left[1 + \eta + \tfrac{1}{2}\eta^2\right]e^{-\eta}, \tag{2a}$$

$$P_m = 1 - A\left[1 + \eta + \tfrac{1}{2}\eta^2\right]e^{-\eta}. \tag{2b}$$

We fit experimental data using this model and obtain the temperature of single atoms as $T_a = 21 \pm 1\ \mu$K, which is consistent with the experimental result of $T_a = 22 \pm 1\ \mu$K by using the release and recapture technique [39]. From the fitted parameters, the factor of $A = 0.94 \pm 0.01$ is extracted. It can be interpreted that most of single atoms remain in the original location if the depth of the moving tweezer is equal to the static one. This fact results from slight differences in the waist of two traps.

The original trap is not switched off or moved to another location, meaning that the entire lattice is not influenced by the transfer process. Therefore, this scheme is suitable for a scalable quantum system. To demonstrate its performance, we prepare a ring optical lattice with three sites and successfully transfer single atoms among these wells. After being initially trapped in site a, one atom is transported to site b and site c in sequence [Fig. 2(b)]. The final probability of single atoms observed in site c is $80 \pm 5\%$ due to the lower depth. In our lattice, the depth of each site is slightly unbalanced. If the total laser power is not sufficient, a single atom trapped in the lowest site is easily lost.

B. Quantum state tomography

Quantum state tomography is a singularly useful tool for reconstructing the density matrices of quantum states [40,41]. It allows the extraction of relevant quantum information quantities such as qubit fidelities and the degrees of entanglement. For one qubit with two levels, tomography requires measuring the three orthogonal components of the Bloch vector. Therefore, to monitor the change during the transfer, a quantum state is detected (1) directly, (2) after applying a $\pi/2$ pulse, (3) after applying a $\pi/2$ pulse with a $\pi/2$ phase shift. The populations of the selected state are denoted by P_1, P_2, and P_3. In the Bloch sphere, the density matrix of an arbitrary state can be written as

$$\rho(p,\theta,\varphi) = \frac{1}{2}\begin{pmatrix} 1 + p\cos\theta & pe^{-i\varphi}\sin\theta \\ pe^{i\varphi}\sin\theta & 1 - p\cos\theta \end{pmatrix}, \tag{3}$$

which is a pure state for the parameter $p = 1$, while for $p < 1$ it is mixed. We define the matrices

$$\mathbf{U}_r(\theta,\varphi) = \begin{pmatrix} \cos\theta/2 & -ie^{-i\varphi}\sin\theta/2 \\ -ie^{i\varphi}\sin\theta/2 & \cos\theta/2 \end{pmatrix}, \tag{4}$$

$$\mathbf{U}_z(\delta,t) = \begin{pmatrix} e^{i\delta t/2} & 0 \\ 0 & e^{-i\delta t/2} \end{pmatrix}. \tag{5}$$

They describe the action of a Raman pulse and the free precession with frequency δ. After applying a Raman pulse, quantum state evolves as $\rho' = \mathbf{U}_r \rho \mathbf{U}_r^\dagger$. For our detection, population in the state $|0\rangle$ is given by the trace as $P = \mathrm{Tr}(\rho' \rho_0)$, where $\rho_0 \equiv \rho\,(p = 1, \theta = 0, \varphi = 0)$. The measurement populations at time T are thus expressed as

$$P_1 = \mathrm{Tr}(\rho\rho_0) = \frac{1}{2}(1 + p\cos\theta), \tag{6a}$$

$$P_2 = \mathrm{Tr}\left(\left[\mathbf{U}_r\left(\frac{\pi}{2}, 0\right)\rho\mathbf{U}_r^\dagger\left(\frac{\pi}{2}, 0\right)\right]\rho_0\right) = \frac{1}{2}(1 + p\,\sin\theta\,\sin\varphi), \tag{6b}$$

$$P_3 = \mathrm{Tr}\left(\left[\mathbf{U}_r\left(\frac{\pi}{2}, \frac{\pi}{2}\right)\rho\mathbf{U}_r^\dagger\left(\frac{\pi}{2}, \frac{\pi}{2}\right)\right]\rho_0\right) = \frac{1}{2}(1 - p\,\sin\theta\,\cos\varphi). \tag{6c}$$

From these equations, the realistic density matrix is obtained:

$$\rho_{\mathrm{real}} = \begin{pmatrix} P_1 & \left[\frac{1}{2} - P_3\right] + i\left[\frac{1}{2} - P_2\right] \\ \left[\frac{1}{2} - P_3\right] - i\left[\frac{1}{2} - P_2\right] & 1 - P_1 \end{pmatrix}. \tag{7}$$

Its fidelity is determined as $F = \mathrm{Re}\,[\mathrm{Tr}\,(\rho_{\mathrm{ideal}}\rho_{\mathrm{real}})]$, where the former represents the ideal density matrix at the measurement time T. When we initialize a single qubit in the state $|1\rangle$, its ideal density matrix is $\rho_1 \equiv \rho\,(p = 1, \theta = \pi, \varphi = 0)$. The fidelity of the eigenstate is thus $F_{\mathrm{eigen}} = 1 - P_1$. When one qubit is initialized in the superposition state $(|1\rangle - i|0\rangle)/\sqrt{2}$, it subsequently undergoes the free precession in the Bloch sphere. For quantum state tomography at time T, we insert an additional π pulse at $T/2$ to reverse inhomogeneous dephasing. As a result, its ideal density matrix is derived from these operations, giving rise to the fidelity of $F_{\mathrm{super}} = 1 - P_2$.

Based on the above calculations, we perform quantum state tomography to investigate the effects of the transfer process. Experimental steps and time sequence are depicted in Figs. 1(b) and 1(c). The moving tweezer ($U_1/k_B = 0.63$ mK) is initially overlapped with the static trap ($U_0/k_B = 0.52$ mK) and always switched on. Once one atom is captured by the combined trap, we initialize an atomic qubit in the state $|1\rangle$ or $(|1\rangle - i|0\rangle)/\sqrt{2}$. It follows the moving tweezer to another location over a distance of 10 μm for a duration time t, and then is transported back under the same conditions. After the round trip, three orthogonal components are detected to reconstruct the density matrix at time T. In the measurement of the superposition state, a π pulse is applied at time $T/2$ when the qubit is transported successfully and located in the moving tweezer. For comparison, density matrices of single atoms in the original location are reconstructed at time $T = 20$ ms,

$$\rho_{\mathrm{eigen}} = \begin{pmatrix} 0.06 \mp 0.02 & 0.02 \pm 0.05 \\ 0.02 \pm 0.05 & 0.94 \pm 0.02 \end{pmatrix} + i\begin{pmatrix} 0 & 0.08 \pm 0.05 \\ -0.08 \mp 0.05 & 0 \end{pmatrix}, \tag{8a}$$

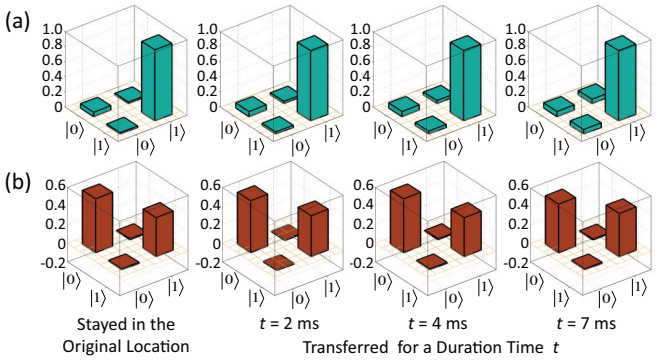

FIG. 3. (Color online) Partial quantum state tomography of single atoms stayed in the original location and transferred to the destination. Real parts of the density matrices for the eigenstate (a) and the superposition state (b) are reconstructed at time $T = 20$ ms. The corresponding transfer duration times are $t = 2$, 4, and 7 ms.

$$\rho_{\mathrm{super}} = \begin{pmatrix} 0.58 \mp 0.04 & 0.01 \pm 0.01 \\ 0.01 \pm 0.01 & 0.42 \pm 0.04 \end{pmatrix} + i\begin{pmatrix} 0 & 0.24 \pm 0.01 \\ -0.24 \mp 0.01 & 0 \end{pmatrix}. \tag{8b}$$

According to the above results, the eigenstate fidelity is $F_{\mathrm{eigen}} = 0.94 \pm 0.02$. The loss results from the imperfections of state preparation and detection. However, for the superposition state, the value is $F_{\mathrm{super}} = 0.74 \pm 0.01$ at time $T = 20$ ms. The rapid loss of fidelity represents homogeneous dephasing due to the instabilities of the surrounding environment. Meanwhile, we measure density matrices during the transfer of single qubits. In our experiment, the distance from the original location to the destination is constant. The duration time is set at $t = 2$, 3, 4, 5, 6, and 7 ms and thus determines the mean transfer velocity of single atoms. The mean velocity is slowed when we prolong the duration time. As shown in Fig. 3, examples of density matrices are reconstructed. Qubit fidelities are recorded in Fig. 4, where the superposition fidelities at time $T = 12$ ms and $T = 20$ ms are presented simultaneously. The dashed lines represent the values without the transfer process. It is observed that the eigenstate fidelity can be well preserved, while the superposition state is affected by the transfer. This influence is decreased with slowing the transfer velocity, but still exists.

C. Spin-echo measurement

In order to obtain the temporal evolutions of the quantum state during the transfer process, a complete state tomography requires plenty of measurements at different times. It is thus a suitable way to investigate coherence properties utilizing spin-echo technique. In this technique, an additional π pulse is inserted at time $T/2$ between two $\pi/2$ pulses to reverse inhomogeneous dephasing [12,42]. Visibilities for different spin-echo fringes are decreased if the time T between $\pi/2$ pulses is extended. We extract the homogeneous dephasing time T_2' from a Gaussian fit

$$V_{\mathrm{spin\ echo}}(t) = V_0 \exp\left(-\frac{t^2}{T_2'^2}\right). \tag{9}$$

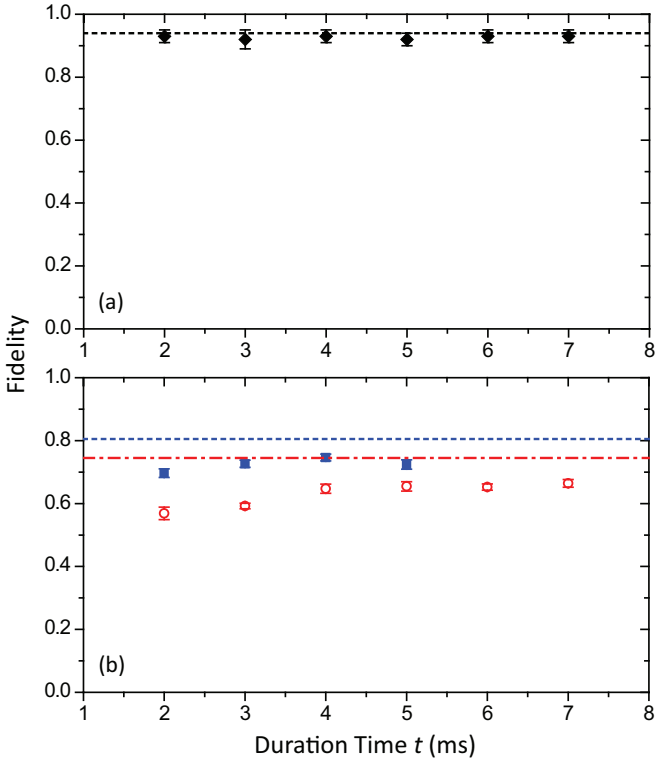

FIG. 4. (Color online) Qubit fidelities as a function of the transfer duration time. The dashed lines represent values without the transfer. (a) The eigenstate fidelities are well preserved in the whole transfer process. (b) For the superposition state, fidelities are detected at time $T = 20$ ms (open circle) and $T = 12$ ms (solid square). The influence on qubit fidelity is weakened with the prolongation of duration time but still exists.

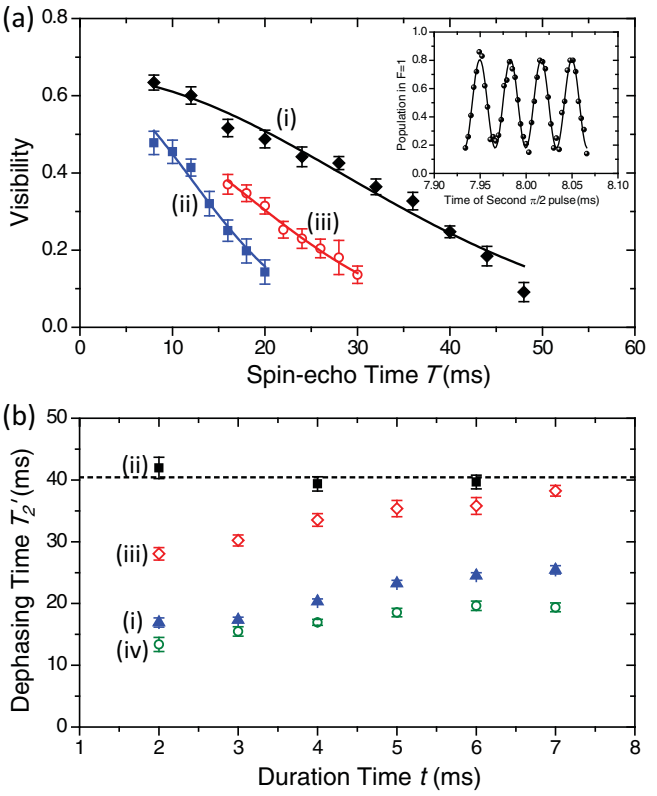

FIG. 5. (Color online) (a) Examples of spin-echo visibilities as a function of different measurement time. The inset shows spin-echo fringes at time $T = 8$ ms without the transfer, which are plotted as a function of time of the second $\pi/2$ pulse around T. All the visibilities are extracted from the corresponding measurement fringes and fitted with a Gaussian depicted in Eq. (9). Without the transfer, the homogeneous dephasing time is $T_2' = 40.4 \pm 1.4$ ms [(i), solid diamond]. For the transfer times $t = 2$ ms and $t = 7$ ms, the values are $T_2' = 16.9 \pm 0.8$ ms [(ii), solid square] and $T_2' = 25.5 \pm 0.7$ ms [(iii), open circle]. (b) Homogeneous dephasing time for different variations of the traps. The dashed line represents the result without any change. Our transfer scheme is performed [(i), solid triangle]. One atom is trapped in an individual tweezer and transported [(ii), solid square]. The depth of one trap is varied gradually [(iii), open diamond]. A tweezer with shallow depth crosses a static trap, meaning that single atoms remain in the initial location [(iv), open circle].

This spin-echo process is similar to the second tomographic measurement of the superposition state, which allows us to obtain the fidelity $F_{\text{super}} = 1 - P_2$. The decreases of spin-echo visibilities are in accordance with the situations of qubit fidelities. Therefore, the measured dephasing time T_2' represents the fidelity properties.

As shown in Fig. 1(b), the steps for spin-echo measurement are described below in detail. (i) After trapping one atom in the static trap overlapped with the moving tweezer, we initialize qubit in the state $|1\rangle$ and then apply a $\pi/2$ pulse. (ii) The atom is transferred to another location over a distance of 10 μm within a duration time t. (iii) When the transport is finished, a π pulse is applied in the middle of the measurement process at time $T/2$. (iv) The atom is transported back for the same duration time. (v) Finally, we apply the second $\pi/2$ pulse around T and plot the spin-echo fringes. Examples of the visibilities as a function of different measurement time T are shown in Fig. 5(a). From the fitted parameters according to Eq. (9), the dephasing time without transferring is extracted as $T_2' = 40.4 \pm 1.4$ ms. It is lowered to $T_2' = 16.9 \pm 0.8$ ms and $T_2' = 25.5 \pm 0.7$ ms when the qubit is transferred for duration times $t = 2$ ms and $t = 7$ ms. For the longer duration time, the mean transfer velocity of single atoms is slower. The influence on dephasing time is thus weakened gradually, which is in accordance with the result of the tomographic measurement.

During the transfer process, the combined trap depth is varied because the tweezer moves across the static trap. In order to investigate the influence factors, we perform different variations of the trap for comparison. First of all, one atom is trapped in an individual tweezer without the lattice and moved to the same destination. In the spin-echo measurement, coherence properties are not influenced by this motion. Secondly, we ramp down the depth of one trap and then ramp up the depth. Spin-echo measurement is performed similarly. For a duration time $t = 7$ ms, the dephasing time is close to the value without the variation. However, the loss of coherence appears for the shorter duration time. Finally, the depth of the moving tweezer is set lower than the static trap. When the tweezer moves across, single atoms are not transferred and remain in the original location, as deduced from Fig. 2(a). In this process, coherence properties are affected.

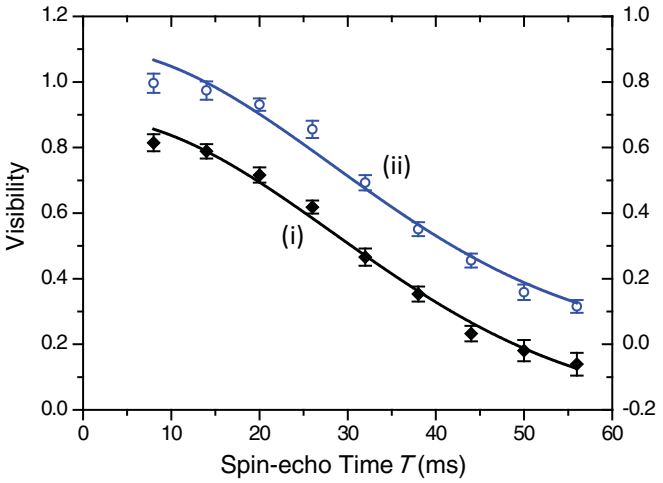

FIG. 6. (Color online) Spin-echo visibilities as a function of different measurement time for one atom in a neighboring site. One atom is transferred from the original site a to the target site b by using the moving tweezer. During the transfer process, spin-echo technique is applied for another one trapped in the neighboring site c. We fit the visibilities with a Gaussian. All the data are plotted in the figure with two vertical axes. Without the transfer process, the homogeneous dephasing time of one atom in a neighboring site is $T_2' = 40.1 \pm 1.1$ ms [(i), solid diamond, corresponding to the left axis]. For the transfer duration time $t = 2$ ms, the dephasing time is $T_2' = 39.9 \pm 1.3$ ms [(ii), open circle, corresponding to the right axis].

For these comparison experiments, the optical potential depth is equal to the value of the transfer process. From the results recorded in Fig. 5(b), several important features can be noticed. (1) The motion of an individual tweezer cannot affect the coherence properties. (2) The more serious loss of coherence is observed for the shorter duration time. (3) The influence of this transfer process is mainly due to the movement across the static trap, rather than the depth variation.

D. Coherence in a neighboring site

Our transfer scheme is appropriate for scalable quantum registers because of no need to change the other sites of the lattice. During the transfer process, we investigate the influence on coherence of another atom in a neighboring site. The moving tweezer is overlapped with the original site a. Similar to above, the trap depth of each site and the tweezer is $U_0/k_B = 0.52$ mK and $U_1/k_B = 0.63$ mK, respectively. Once single atoms are captured in site a and its neighboring site c at the same time, the experimental sequence depicted in Fig. 1(c) is performed. After preparation of the initial state, one atom in site a is transferred to the target site b and then transported back. Meanwhile, the spin-echo technique is applied for the other atom in site c. As shown in Fig. 6, visibilities of spin-echo fringes are fitted with a Gaussian. Without the transfer, we obtain the homogeneous dephasing time in the neighboring site c as $T_2' = 40.1 \pm 1.1$ ms. When one atom is transferred from site a to site b for duration time $t = 2$ ms, the dephasing time in site c is $T_2' = 39.9 \pm 1.3$ ms. A comparison between both measurement results shows that they are in reasonable agreement. Therefore, coherence properties of single atoms in a neighboring site are not influenced by the transfer process.

III. ANALYSIS OF DEPHASING MECHANISMS

In this section, we analyze and discuss the homogeneous dephasing mechanisms. Since the dephasing time represents the fidelity properties of single qubits, the influences of the transfer process on fidelities are illustrated simultaneously. After applying a $\pi/2$ pulse in the spin-echo measurement, the free evolution frequency $\delta = \omega_R - \omega_0$ is the detuning of the two-photon Raman pulse with frequency ω_R from the atomic resonance ω_0. For one atom located in the trap, the detuning is given by [43]

$$\delta = \omega_R - \omega_{hfs} - \delta_{ac} - \delta_B, \tag{10}$$

where $\omega_{hfs} = 2\pi \times 6.834$ GHz is the hyperfine splitting of the ground state without any fields, δ_{ac} is the difference of ac Stark shifts between hyperfine levels induced by the trap laser, and δ_B is the quadratic Zeeman shift of the bias magnetic field. In the presence of field fluctuations and motions of single atoms, the time-dependent evolution frequencies result in a finite coherence time. Common dephasing mechanisms are thus the intensity fluctuations of the trap laser, the beam pointing instabilities, heating effects of single atoms, and the bias magnetic field fluctuations. As listed in Table I, these factors are detected and estimated in detail.

A. Intensity fluctuations of the trap laser

The intensity noises of the trap laser result in the fluctuations of the differential ac Stark shift. Due to the large detuning of the laser with an effective value $\Delta_{eff} = 2\pi \times 20.0$ THz [44], the differential light shift is approximated as $\hbar\delta_{ac} = \eta U$, where a scaling factor η is identified as $\eta = \omega_{hfs}/\Delta_{eff}$. We derive the following expression:

$$\delta_{ac} = \delta_{ac0} + \frac{\eta \Delta U}{\hbar}, \tag{11}$$

where δ_{ac0} is the value without any fluctuations, and ΔU represents the influence of intensity noise. The varied evolution frequency is given by

$$\Delta\delta = \delta_{ac} - \delta_{ac0} = \frac{\eta U \sigma_{inten}}{\hbar}, \tag{12}$$

with $\sigma_{inten} = dI/I$. In the spin-echo measurement, we define the dephasing time as

$$T_2' = \frac{2}{\Delta\delta/2\pi}, \tag{13}$$

where the factor of 2 arises because T represents the time between two $\pi/2$ pulses. In order to obtain the intensity fluctuations of the static trap and the moving one, we shine laser beams onto a photodiode and record the powers for a duration time of 2 s. From the signals, we calculate the relative intensity noise as $\sigma_{inten} \simeq 0.001$. The induced dephasing time is $T_2' \simeq 245$ ms.

TABLE I. Summary of homogeneous dephasing mechanisms in the experiment. Values are listed with the transfer for duration times $t = 2$ ms, $t = 7$ ms, and without the transfer. The combined dephasing time is calculated from $1/T_2' = \sum_n 1/T_{2,n}'$ with each evaluation result $T_{2,n}'$. Here, the depths of the static trap and the moving one are $U_0/k_B = 0.52$ mK and $U_1/k_B = 0.63$ mK, respectively. The bias magnetic field is $B_0 = 2$ G.

			Dephasing time T_2' (ms)		
			Without transferring	With transferring	
Sections	Mechanisms	Parameters		$t = 2$ ms	$t = 7$ ms
II C	Experimental results		40.4 ± 1.4	16.9 ± 0.8	25.5 ± 0.7
III A	Intensity fluctuations	$\sigma_{\text{inten}} \simeq 0.001$	245	245	245
III B	Pointing instabilities	$\sigma_{\text{point}} \simeq 0.06$	68	31	31
III C	Heating effects	$\langle\dot{\varepsilon}\rangle/k_B \simeq 20\ \mu$K/s	704	$\ll 704$	704
III D	Magnetic field fluctuations	$\sigma_B \simeq 0.001$	1750	1750	1750
	Combined		48	< 26	26

B. Pointing instabilities of the trap laser

The pointing instabilities result from variations of the optical paths. Their maximum frequency is much lower than the radial oscillation frequency of trapped atoms. We can make a strong assumption that atoms always follow the pointing variations of the trap laser. However, in our experiment single atoms are captured by the overlapped trap of two laser beams, each beam with individual pointing noise. Therefore, the differential light shift is affected by the variations of the relative position between two lasers. Without the transfer of single atoms, we calculate the varied depth as

$$\Delta U = \tfrac{1}{2} m\omega_r^2 dx^2, \tag{14}$$

where $\omega_r = \sqrt{4U/mw_0^2}$ is the radial oscillation frequency of single atoms, w_0 is the waist of the strongly focused laser, and dx is the relative position between two lasers induced by these instabilities. In our experiment, the radial oscillation frequency is $\omega_r = 2\pi \times 48.0$ kHz for the combined trap. For a normalized pointing noise $\sigma_{\text{point}} = dx/w_0$, Eq. (14) is written as

$$\Delta U = 2U\sigma_{\text{point}}^2. \tag{15}$$

The variation of the detuning is given by

$$\Delta\delta = \delta_{\text{ac}} - \delta_{\text{ac0}} = \frac{2\eta U\sigma_{\text{point}}^2}{\hbar}. \tag{16}$$

According to the method in Ref. [43], we measure the point instabilities. One laser beam is divided into two parts and then detuned by $\omega_0 = 2\pi \times 80.00$ MHz and $\omega_1 = 2\pi \times 80.01$ MHz, respectively. After propagating along independent optical paths, they are overlapped partially and shined on a photodiode. We record the powers during a duration time of 2 s and calculate the temporal amplitudes of the beat signals with frequency $\Delta\omega = 2\pi \times 10$ kHz using a fast Fourier transform algorithm. Amplitude variations dA/A reflect the pointing fluctuations σ_{point}. For the time scales $t \leqslant 100$ ms, the fluctuations can reach up to 0.06. The dephasing time is calculated as $T_2' \simeq 68$ ms.

While we move the optical tweezer and perform our transfer process, the relative position between two laser beams is increased by a distance from 0 to 10 μm. For one atom, the transfer to the deeper tweezer is achieved when $\Delta x = x_a$, where $x_a = w_0\sqrt{k_B T_a/4U}$ is the extension of the atomic wave function. Then, the atom is trapped in the individual tweezer and transported to the destination. Coherence properties are not affected by the pointing instabilities when the relative position is larger than x_a, implying that an average distance of $\langle\Delta x\rangle = x_a/2$ is used for the corresponding calculation. The varied depth due to the pointing instabilities is thus extended to

$$\begin{aligned}\Delta U_{\text{tran}} &= \tfrac{1}{2} m\omega_r^2(\langle\Delta x\rangle + dx)^2 - \tfrac{1}{2} m\omega_r^2\langle\Delta x\rangle^2 \\ &= (1+\xi)\Delta U,\end{aligned} \tag{17}$$

where $\xi = 2\langle\Delta x\rangle/dx$ is a scaling factor. On our condition of $x_a/w_0 \simeq 0.07$, $\xi \simeq 1.17$ is obtained. Therefore, the dephasing time is $T_2' \simeq 31$ ms during the transfer process, meaning that this effect is more obvious.

C. Heating effects of single atoms

In the spin-echo measurement, heating effects of single atoms also result in homogeneous dephasing. It is due to the different light shifts between twice free evolution processes. Taking into account harmonic oscillations of atoms and the energy distributions, the average differential light shift is expressed as $\delta_{\text{ac}}(E) = \delta_0 + \eta E/2\hbar$ [43]. Here, δ_0 is the maximum differential light shift and $E/2$ is the average potential energy. We assume that there is an average energy gain of ΔE for the subsequent evolution process in comparison with the first one. The corresponding variation of the differential light shift is given by

$$\Delta\delta = \delta_{\text{ac}}(E + \Delta E) - \delta_{\text{ac}}(E) = \frac{\eta\Delta E}{2\hbar}. \tag{18}$$

Our experimental heating effects have been investigated in detail [45]. Owing to laser fluctuations and photon scattering, the average heating rate is $\langle\dot{\varepsilon}\rangle/k_B \simeq 20\ \mu$K/s. The energy gain is obtained as $\Delta E/k_B = \langle\dot{\varepsilon}\rangle/k_B\,(T/2) \simeq 0.4\ \mu$K for the time $T = 40$ ms. According to Eq. (13), we calculate the dephasing time $T_2' \simeq 704$ ms, which is much larger than the spin-echo time.

During the transfer, additional heating effects need to be considered. On the one hand, single atoms gain momentum in this process. It is adiabatic if the transfer acceleration

a fulfills $max_a \ll h\nu_r$, where $\nu_r = \omega_r/2\pi$, and x_a is the extension of the wave function depicted in Sec. III B [19,46]. Our transfer scheme via the PZT gives a typical acceleration of $a \simeq 20\ \mathrm{m/s^2}$. The corresponding adiabatic condition is thus satisfied, which can be proved by the transport results in an individual tweezer. On the other hand, the trap depth is varied at the same time. The adiabatic conditions for changes in the oscillation frequencies are $d\nu_r/dt \ll \nu_r^2$ and $d\nu_z/dt \ll \nu_z^2$, where ν_r and ν_z represent the radial and axial oscillations, respectively [19]. In our situation, oscillation frequencies are $\nu_r = 48.0$ kHz and $\nu_z = 4.1$ kHz for the combined trap. Therefore, $\nu_r^2 \simeq 2.3 \times 10^9\ \mathrm{Hz^2}$ and $\nu_z^2 \simeq 1.7 \times 10^7\ \mathrm{Hz^2}$ are calculated. In the radial direction, we obtain $d\nu_r/dt \simeq 0.4 \times 10^9$, $0.1 \times 10^9\ \mathrm{Hz^2}$ when the transfer time is $t = 2$, 7 ms. Similarly, the corresponding results are $d\nu_z/dt \simeq 3.5 \times 10^7$, $0.1 \times 10^7\ \mathrm{Hz^2}$ in the axial direction. These estimates illustrate the transition from a nonadiabatic to an adiabatic transfer process. From the experimental results in Fig. 5(b), we obtain that the dephasing time increases with the prolongation of the duration time, and finally keeps a constant value. It is thus deduced that heating effects induced by the transfer can be ignored for a long duration time. In Table I, we assume that the corresponding dephasing time is kept at $T_2' \simeq 704$ ms for $t = 7$ ms. However, heating effects induced by the transfer process cause a serious loss of qubit fidelity for $t = 2$ ms.

D. Fluctuations of the bias magnetic field

A bias magnetic field of $B_0 = 2$ G is applied to generate the quantization axis. The fluctuations of this field directly affect the evolution frequency, and thus the homogeneous dephasing time. According to the Breit-Rabi formula, the second-order Zeeman shift of the energy is written as

$$\Delta E_{F=3/2\pm1/2,m_F=0}(B) = -\frac{\hbar\omega_{\mathrm{hfs}}}{6} \pm \frac{\hbar\omega_{\mathrm{hfs}}}{2}\left[1 + \frac{(g_J - g_I)^2\mu_{\mathrm{B}}^2 B^2}{\hbar^2\omega_{\mathrm{hfs}}^2}\right]^{1/2}, \quad (19)$$

where μ_{B} is the Bohr magneton, and $g_J = 1$, $g_I \simeq 0.001$ are the electron spin and nuclear Landé factors. The differential energy between the states $|0\rangle$ and $|1\rangle$ reads

$$U(B) = \Delta E_{F=2,m_F=0}(B) - \Delta E_{F=1,m_F=0}(B). \quad (20)$$

By taking the derivative of this equation at $B = B_0$, we obtain

$$\Delta U = \beta\hbar\omega_{\mathrm{hfs}}\frac{\Delta B}{B_0}, \quad (21)$$

with

$$\beta = \left[1 + \frac{(g_J - g_I)^2\mu_{\mathrm{B}}^2 B_0^2}{\hbar^2\omega_{\mathrm{hfs}}^2}\right]^{-1/2}\frac{(g_J - g_I)^2\mu_{\mathrm{B}}^2 B_0^2}{\hbar^2\omega_{\mathrm{hfs}}^2}. \quad (22)$$

In our experiment, $\beta = 1.7 \times 10^{-7}$ is calculated. The varied evolution frequency due to the magnetic field fluctuations is derived by

$$\Delta\delta = \frac{\Delta U}{\hbar} = \beta\omega_{\mathrm{hfs}}\sigma_{\mathrm{B}}, \quad (23)$$

where $\sigma_{\mathrm{B}} = \Delta B/B_0$ is the relative magnetic fluctuation. We conservatively estimate that $\sigma_{\mathrm{B}} \simeq 0.001$ is feasibly achieved with an application of precision current source. This effect results in a rather long time of $T_2' \simeq 1750$ ms.

IV. DISCUSSIONS AND CONCLUSION

In conclusion, we have demonstrated the transfer of a single ^{87}Rb atom among the sites of a ring optical lattice with an auxiliary moving tweezer. The transfer efficiency of single atoms has been observed to increase as the depth ratio between the moving tweezer and the static trap. It gives the maximum efficiency of $95 \pm 5\%$ when the ratio is greater than 1.2 in our conditions. Similarly, for small atomic ensembles, the number of transferred atoms increases with the depth ratio [26]. For explanation, we make an assumption that an atom with energy smaller than the differential depth is trapped in the moving tweezer. The obtained temperature of single atoms is consistent with the measurement result via the release and recapture technique. Meanwhile, the density matrix has been reconstructed by performing partial quantum state tomography. Qubit fidelity of the eigenstate can be well preserved during the transfer process, while the fidelity of the superposition state is lost. By applying spin-echo measurement, we have obtained the homogeneous dephasing time and analyzed the influence mechanisms in detail. When the duration time is short, heating effects induced by the transfer cause the serious loss of qubit fidelity. For a long duration time, the loss of fidelity is mainly due to the pointing instabilities of laser beams. This finding is supported by our estimated results in Table I. The combined dephasing times are $T_2' \simeq 48$ ms without the transfer and $T_2' \simeq 26$ ms for the transfer time $t = 7$ ms. During the transfer, laser pointing fluctuations can be suppressed by reducing the voltage noise imposed on the PZT and operating the PZT in the closed-loop mode. Moreover, the optical dipole trap laser with larger detuning or magic wavelength may be chosen. We can thus improve coherence time during this process in the future.

In the previous investigations of transport, the reduction of coherence with an "optical conveyor belt" is explained by the heating effects [22]. During an alternate transfer between two moving tweezers, the coherence of single atoms is not affected by this process [23]. However, these schemes are not suitable for scalable quantum systems as the original well is switched off or moved simultaneously during the transport. The transfer using auxiliary optical tweezers as demonstrated in this work would not affect single qubits in other sites of the lattice, including its location in the trap and coherence properties. In comparison with single ions, as depicted in Table II, there exist many challenges for single neutral atoms, including increasing success probability and qubit fidelity during the transfer and achieving the fast transport. These requirements may need to combine our scheme with alternative methods; for instance, Raman sideband cooling [47]. If single atoms are cooled to the vibrational ground state of the optical potential, the optimal nonadiabatic transport process will be performed [19,48].

A complete architecture for scalable quantum computation in an optical lattice has been proposed and theoretically investigated in Ref. [19]. On the basis of quantum register

TABLE II. Comparisons between single neutral atoms and atomic ions transport processes. Here, we perform the transport of single atoms in an optical lattice by using an auxiliary moving tweezer with deeper trap depth. For single ions, multizone electric trap arrays are used for scalable quantum computation. Previously, ion shuttling between storage and interaction regions has been investigated in detail. Their common requirements include high efficiency, minimal energy gain, maintained qubit coherence, and minimal transport time.

	Single neutral atoms	Single atomic ions
Transport region	From remote sites into interaction range	Between storage and interaction regions
Method	Auxiliary moving tweezer	Time-dependent electric potential
Efficiency	$\simeq 0.95$[a]	$\simeq 1$[b]
Energy gain	Adiabatic transport	Adiabatic transport[c]/sympathetically cooling[d]/ electric field noise[e]
Qubit coherence	Laser pointing fluctuations	Magnetic field fluctuations[f]
Operation time	Optimal nonadiabatic transport[g]	Optimal nonadiabatic transport[h]

[a]This work.
[b]Reference [30].
[c]Reference [30].
[d]References [31,32].
[e]Reference [33].
[f]Reference [33].
[g]Reference [47].
[h]References [34,35].

preparation, two selected qubits are transported to neighboring sites using moving optical tweezers. Utilizing collisional interactions between atoms, three different two-qubit gates have been discussed in detail. In the architecture for scalable quantum computation, application of our work is anticipated.

ACKNOWLEDGMENTS

This work was supported by the National Basic Research Program of China under Grant No. 2012CB922101, the National Natural Science Foundation of China under Grants No.11104320 and No. 11104321, and funds from the Chinese Academy of Sciences.

[1] D. DiVincenzo, Fortschr. Phys. **48**, 771 (1998).
[2] T. D. Ladd, F. Jelezko, R. Laflamme, Y. Nakamura, C. Monroe, and J. L. O'Brien, Nature (London) **464**, 45 (2010).
[3] U. Dorner, T. Calarco, P. Zoller, A. Browaeys, and P. Grangier, J. Opt. B: Quantum Semiclass. Opt. **7**, S341 (2005).
[4] D. Schrader, I. Dotsenko, M. Khudaverdyan, Y. Miroshnychenko, A. Rauschenbeutel, and D. Meschede, Phys. Rev. Lett. **93**, 150501 (2004).
[5] I. Bloch, Nature (London) **453**, 1016 (2008).
[6] W. S. Bakr, A. Peng, M. E. Tai, R. Ma, J. Simon, J. I. Gillen, S. Fölling, L. Pollet, and M. Greiner, Science **329**, 547 (2010).
[7] J. F. Sherson, C. Weitenberg, M. Endres, M. Cheneau, I. Bloch, and S. Kuhr, Nature (London) **467**, 68 (2010).
[8] P. Würtz, T. Langen, T. Gericke, A. Koglbauer, and H. Ott, Phys. Rev. Lett. **103**, 080404 (2009).
[9] C. Weitenberg, M. Endres, J. F. Sherson, M. Cheneau, P. Schauß, T. Fukuhara, I. Bloch, and S. Kuhr, Nature (London) **471**, 319 (2011).
[10] M. Khudaverdyan, W. Alt, I. Dotsenko, L. Förster, S. Kuhr, D. Meschede, Y. Miroshnychenko, D. Schrader, and A. Rauschenbeutel, Phys. Rev. A **71**, 031404 (2005).
[11] D. D. Yavuz, P. B. Kulatunga, E. Urban, T. A. Johnson, N. Proite, T. Henage, T. G. Walker, and M. Saffman, Phys. Rev. Lett. **96**, 063001 (2006).
[12] S. Yu, P. Xu, X. D. He, M. Liu, J. Wang, and M. S. Zhan, Opt. Express **21**, 32130 (2013).
[13] T. Wilk, A. Gaëtan, C. Evellin, J. Wolters, Y. Miroshnychenko, P. Grangier, and A. Browaeys, Phys. Rev. Lett. **104**, 010502 (2010).
[14] L. Isenhower, E. Urban, X. L. Zhang, A. T. Gill, T. Henage, T. A. Johnson, T. G. Walker, and M. Saffman, Phys. Rev. Lett. **104**, 010503 (2010).
[15] M. Saffman, T. G. Walker, and K. Mølmer, Rev. Mod. Phys. **82**, 2313 (2010).
[16] D. Jaksch, H.-J. Briegel, J. I. Cirac, C. W. Gardiner, and P. Zoller, Phys. Rev. Lett. **82**, 1975 (1999).
[17] O. Mandel, M. Greiner, A. Widera, T. Rom, T. W. Hänsch, and I. Bloch, Nature (London) **425**, 937 (2003).
[18] M. Anderlini, P. J. Lee, B. L. Brown, J. Sebby-Strabley, W. D. Phillips, and J. V. Porto, Nature (London) **448**, 452 (2007).
[19] C. Weitenberg, S. Kuhr, K. Mølmer, and J. F. Sherson, Phys. Rev. A **84**, 032322 (2011).
[20] O. Mandel, M. Greiner, A. Widera, T. Rom, T. W. Hänsch, and I. Bloch, Phys. Rev. Lett. **91**, 010407 (2003).
[21] A. Steffen, A. Alberti, W. Alt, N. Belmechri, S. Hild, M. Karski, A. Widera, and D. Meschede, Proc. Natl. Acad. Sci. USA **109**, 9770 (2012).
[22] S. Kuhr, W. Alt, D. Schrader, I. Dotsenko, Y. Miroshnychenko, W. Rosenfeld, M. Khudaverdyan, V. Gomer, A. Rauschenbeutel, and D. Meschede, Phys. Rev. Lett. **91**, 213002 (2003).

[23] J. Beugnon, C. Tuchendler, H. Marion, A. Gaëtan, Y. Miroshnychenko, Y. R. P. Sortais, A. M. Lance, M. P. A. Jones, G. Messin, A. Browaeys, and P. Grangier, Nat. Phys. **3**, 696 (2007).
[24] A. Lengwenus, J. Kruse, M. Schlosser, S. Tichelmann, and G. Birkl, Phys. Rev. Lett. **105**, 170502 (2010).
[25] J. Kruse, C. Gierl, M. Schlosser, and G. Birkl, Phys. Rev. A **81**, 060308(R) (2010).
[26] M. Schlosser, J. Kruse, C. Gierl, S. Teichmann, S. Tichelmann, and G. Birkl, New J. Phys. **14**, 123034 (2012).
[27] S. Yu, X. D. He, P. Xu, M. Liu, J. Wang, and M. S. Zhan, Chin. Sci. Bull. **57**, 1931 (2012).
[28] M. J. Piotrowicz, M. Lichtman, K. Maller, G. Li, S. Zhang, L. Isenhower, and M. Saffman, Phys. Rev. A **88**, 013420 (2013).
[29] F. Nogrette, H. Labuhn, S. Ravets, D. Barredo, L. Béguin, A. Vernier, T. Lahaye, and A. Browaeys, Phys. Rev. X **4**, 021034 (2014).
[30] M. A. Rowe, A. Ben-Kish, B. Demarco, D. Leibfried, V. Meyer, J. Beall, J. Britton, J. Hughes, W. M. Itano, B. Jelenković, C. Langer, T. Rosenband, and D. J. Wineland, Quantum Inf. Comput. **2**, 257 (2002).
[31] J. P. Home, D. Hanneke, J. D. Jost, J. M. Amini, D. Leibfried, and D. J. Wineland, Science **325**, 1227 (2009).
[32] R. B. Blakestad, C. Ospelkaus, A. P. VanDevender, J. M. Amini, J. Britton, D. Leibfried, and D. J. Wineland, Phys. Rev. Lett. **102**, 153002 (2009).
[33] R. B. Blakestad, C. Ospelkaus, A. P. VanDevender, J. H. Wesenberg, M. J. Biercuk, D. Leibfried, and D. J. Wineland, Phys. Rev. A **84**, 032314 (2011).
[34] A. Walther, F. Ziesel, T. Ruster, S. T. Dawkins, K. Ott, M. Hettrich, K. Singer, F. Schmidt-Kaler, and U. Poschinger, Phys. Rev. Lett. **109**, 080501 (2012).
[35] R. Bowler, J. Gaebler, Y. Lin, T. R. Tan, D. Hanneke, J. D. Jost, J. P. Home, D. Leibfried, and D. J. Wineland, Phys. Rev. Lett. **109**, 080502 (2012).
[36] X. D. He, P. Xu, J. Wang, and M. S. Zhan, Opt. Express **17**, 21007 (2009).
[37] P. Xu, X. D. He, J. Wang, and M. S. Zhan, Opt. Lett. **35**, 2164 (2010).
[38] N. Schlosser, G. Reymond, and P. Grangier, Phys. Rev. Lett. **89**, 023005 (2002).
[39] C. Tuchendler, A. M. Lance, A. Browaeys, Y. R. P. Sortais, and P. Grangier, Phys. Rev. A **78**, 033425 (2008).
[40] R. T. Thew, K. Nemoto, A. G. White, and W. J. Munro, Phys. Rev. A **66**, 012303 (2002).
[41] H. F. Hofmann and S. Takeuchi, Phys. Rev. A **69**, 042108 (2004).
[42] M. F. Andersen, A. Kaplan, and N. Davidson, Phys. Rev. Lett. **90**, 023001 (2003).
[43] S. Kuhr, W. Alt, D. Schrader, I. Dotsenko, Y. Miroshnychenko, A. Rauschenbeutel, and D. Meschede, Phys. Rev. A **72**, 023406 (2005).
[44] D. Schrader, S. Kuhr, W. Alt, M. Müller, V. Gomer, and D. Meschede, Appl. Phys. B **73**, 819 (2001).
[45] X. D. He, S. Yu, P. Xu, J. Wang, and M. S. Zhan, Opt. Express **20**, 3711 (2012).
[46] A. Browaeys, H. Häffner, C. McKenzie, S. L. Rolston, K. Helmerson, and W. D. Phillips, Phys. Rev. A **72**, 053605 (2005).
[47] J. D. Thompson, T. G. Tiecke, A. S. Zibrov, V. Vuletić, and M. D. Lukin, Phys. Rev. Lett. **110**, 133001 (2013).
[48] A. Couvert, T. Kawalec, G. Reinaudi, and D. Guéry-Odelin, Europhys. Lett. **83**, 13001 (2008).